AFRL-RZ-WP-TR-2010-2106

PROPULSION AND POWER RAPID RESPONSE RESEARCH AND DEVELOPMENT (R&D) SUPPORT

Deliver Order 0002: Power-Dense, Solid Oxide Fuel Cell Systems: High-Performance, High-Power-Density Solid Oxide Fuel Cells—Materials and Load Control

Stephen W. Sofie, Steven R. Shaw, Peter A. Lindahl, and Lee H. Spangler

Montana State University

APRIL 2010
Final Report

AIR FORCE RESEARCH LABORATORY
PROPULSION DIRECTORATE
WRIGHT-PATTERSON AIR FORCE BASE, OH 45433-7251
AIR FORCE MATERIEL COMMAND
UNITED STATES AIR FORCE

NOTICE AND SIGNATURE PAGE

Using Government drawings, specifications, or other data included in this document for any purpose other than Government procurement does not in any way obligate the U.S. Government. The fact that the Government formulated or supplied the drawings, specifications, or other data does not license the holder or any other person or corporation; or convey any rights or permission to manufacture, use, or sell any patented invention that may relate to them.

This report was cleared for public release by the USAF 88th Air Base Wing (88 ABW) Public Affairs (AFRL/PA) Office and is available to the general public, including foreign nationals. Copies may be obtained from the Defense Technical Information Center (DTIC) (http://www.dtic.mil).

AFRL-RZ-WP-TR-2010-2106 HAS BEEN REVIEWED AND IS APPROVED FOR PUBLICATION IN ACCORDANCE WITH THE ASSIGNED DISTRIBUTION STATEMENT.

*//Signature//

RYAN M. MILLER
Chemical Engineer
Thermal & Electrochemical Branch
Energy/Power/Thermal Division

//Signature//

THOMAS L. REITZ
Branch Chief
Thermal & Electrochemical Branch
Energy/Power/Thermal Division
Propulsion Directorate

This report is published in the interest of scientific and technical information exchange, and its publication does not constitute the Government's approval or disapproval of its ideas or findings.

*Disseminated copies will show "//Signature//" stamped or typed above the signature blocks.

REPORT DOCUMENTATION PAGE

Form Approved
OMB No. 0704-0188

1. REPORT DATE *(DD-MM-YY)*	2. REPORT TYPE	3. DATES COVERED *(From - To)*
April 2010	Final	23 November 2007 – 22 February 2010

4. TITLE AND SUBTITLE
PROPULSION AND POWER RAPID RESPONSE RESEARCH AND DEVELOPMENT (R&D) SUPPORT
Deliver Order 0002: Power-Dense, Solid-Oxide Fuel Cell Systems: High-Performance, High-Power-Density Solid Oxide Fuel Cells—Materials and Load Control

5a. CONTRACT NUMBER
FA8650-08-D-2806-0002

5b. GRANT NUMBER

5c. PROGRAM ELEMENT NUMBER
62203F

6. AUTHOR(S)
Stephen W. Sofie, Steven R. Shaw, Peter A. Lindahl, and Lee H. Spangler

5d. PROJECT NUMBER
3145

5e. TASK NUMBER
22

5f. WORK UNIT NUMBER
314522AN

7. PERFORMING ORGANIZATION NAME(S) AND ADDRESS(ES)

By:
Montana State University
P.O. Box 2460
Bozeman, MT 59717-2460

For:
Universal Technology Corporation
1270 N. Fairfield Road
Dayton, OH 45432-2600

8. PERFORMING ORGANIZATION REPORT NUMBER

9. SPONSORING/MONITORING AGENCY NAME(S) AND ADDRESS(ES)
Air Force Research Laboratory
Propulsion Directorate
Wright-Patterson Air Force Base, OH 45433-7251
Air Force Materiel Command
United States Air Force

10. SPONSORING/MONITORING AGENCY ACRONYM(S)
AFRL/RZPS

11. SPONSORING/MONITORING AGENCY REPORT NUMBER(S)
AFRL-RZ-WP-TR-2010-2106

12. DISTRIBUTION/AVAILABILITY STATEMENT
Approved for public release; distribution unlimited.

13. SUPPLEMENTARY NOTES
Report contains color. PA Case Number: 88ABW-2010-2197; Clearance Date: 22 Apr 2010. Report contains color.

14. ABSTRACT

High-Performance, High-Power-Density Solid Oxide Fuel Cells: Materials - Solid oxide fuel cell electrodes based on catalyst coatings offer substantial potential for creating more effective anode and cathode structures. Infiltrated anodes based on nickel metal can yield finer catalyst phase distribution at volumetric concentrations well below percolation for traditional cermets. The coarsening of nickel after high temperature thermal treatment poses substantial degradation to the deposited structure; therefore, methods of anchoring the nickel metal to the YSZ scaffold have been evaluated to stabilize fine scale electro-catalyst particles. Aluminum titanate was introduced into the porous YSZ anode scaffold to facilitate a step-wise chemical reaction to anchor the nickel metal catalyst. SEM observation of thermally treated nickel infiltrated scaffolds indicates excellent preservation of the nickel network at 800 °C for 100 hours. Electrochemical tests show not only decreased degradation rates, but also increased initial performance levels due to the additive.

High Performance, High-Power-Density Solid Oxide Fuel Cells: Load Control - With currently foreseeable technology, a fuel cell stack capable of supplying the dynamic power requirements for turns, climb, and sprint maneuvers is so heavy as to negate the advantage of using a fuel cell in level flight. This essentially requires the hybridization of the fuel cell using a zero-average power source such as a battery or capacitor. In this report, we discuss the development of an extremely simple hybrid controller that combines the current/voltage characteristics of a battery and fuel cell. This controller could be readily adapted to current fuel cell powered vehicles.

15. SUBJECT TERMS
solid oxide fuel cell, SOFC, solid oxide fuel cell electrodes, SOFC systems, hybrid power systems

16. SECURITY CLASSIFICATION OF:			17. LIMITATION OF ABSTRACT:	18. NUMBER OF PAGES	19a. NAME OF RESPONSIBLE PERSON (Monitor)
a. REPORT	b. ABSTRACT	c. THIS PAGE			Ryan M. Miller
Unclassified	Unclassified	Unclassified	SAR	22	19b. TELEPHONE NUMBER *(Include Area Code)* N/A

TABLE OF CONTENTS

LIST OF FIGURES

Figure **Page**

LIST OF TABLES

Table **Page**

1.0 HIGH PERFORMANCE, HIGH POWER DENSITY SOLID OXIDE FUEL CELLS: MATERIALS

1.1 Summary

The use of fine scale and nano-catalysts for fuel cell applications based on infiltration approaches has the potential to increase performance whilst also decreasing weight. Furthermore, the reduced catalyst content required for infiltration approaches requires less than 10 vol% catalyst as opposed to greater than 50 vol% used in traditional fuel cell anode cermets. The deficit with fine/nano-scale metal catalyst particles is the thermodynamic instability which is exasperated by excessive coarsening at the high temperatures of Solid Oxide Fuel Cell (SOFC) operation. While ceramic catalysts yield promise for improved thermal stability, the relatively poor catalytic performance of these materials reduces overall performance of the SOFC system. The goals of the present study are to establish the methods and effectiveness of anchoring metallic catalysts to the yttria-stabilized zirconia (YSZ) ceramic scaffold for the purposes of preventing nickel coarsening, agglomeration, and break-up of the three-dimensional (3-D) catalyst network that supports electrochemical function through triple phase boundary length and current collection through the bulk portion of the anode. The use of the aluminum titanate has evolved from a coefficient of thermal expansion (CTE) lowering additive in traditional nickel/YSZ cermets to an anchoring additive for infiltrated nickel electro-catalyst. The aluminum titanate anchors have shown to be effective in stabilizing nickel nano-sized catalysts for up to 100 hours at 800 ^{o}C. Improved electrochemical performance is noted with the catalyst anchors and it is anticipated that the chemical anchors will also facilitate catalyst stability under fuel contaminates as well.

1.2 Introduction

Anode supported solid oxide fuel cells have shown the best potential for high power densities due largely to the thin electrolytes, but also due to the catalytic characteristics of nickel as well as the excellent conductivity. The implementation of traditional nickel oxide processed anodes, however, requires in excess of 35 vol% to satisfy full percolation of the catalyst network and hence current collection conduits. Nickel metal is the most cost effective metal used in the anodes to allow the electrons a path through the substrate to where the power can be harnessed. However, large quantities of nickel metal must be mixed with the anode materials in order to thoroughly provide a percolated network.

Infiltration of electro-catalysts offers substantial potential in creating finer metal networks to enhance triple phase boundary length while requiring substantially less catalyst. In addition to finer catalytic structures, benefits in weight and cost can be attained though infiltration in which more exotic catalysts can become viable given the substantially decreased loading. This methodology has several advantages, the first in that the CTE of an infiltrated anode is dictated by the support scaffold, most notably YSZ, and the fabrication of tailored pore structures to reduce diffusion limitations that can yield substantial lag in redox cycling and concentration polarization. In this manner a porous substrate can be infiltrated with a nickel nitrate or other solution precursor to coat the walls of the pores thus creating a 3-D catalyst network and allowing an electron path to the interconnect. Infiltration can also yield better

mechanical performance by allowing more YSZ to remain in the anode. Unfortunately, the nickel metal coarsens rapidly at operational temperatures causing a discontinuous path and decreased triple phase boundary length. In this manner most metal catalysts, in addition to nickel, are currently poor choices for infiltrated anode catalysts.

The objective of this study is to evaluate the use of aluminum titanate to chemically anchor the catalyst on the porous YSZ scaffold. Aluminum titanate anchoring additives would be introduced to the anode substrate and chemically interact with both the substrate and with the infiltrated nickel. This chemical anchoring is intended to reduce the affects of thermally-induced nickel coarsening thus mitigating rapid degradation of fine infiltrated catalysts. The chemical interactions between the metastable aluminum titanate additives and nickel/YSZ will be evaluated by x-ray diffraction (XRD) diffraction as a function of temperature. In addition, microscopy and electrochemical testing will be performed to characterize the effects of the chemical anchors.

1.3 Experimental Procedure

1.3.1 Chemical Reactivity

To evaluate the feasibility of anchors, the chemical interactions of the possible anchors with regard to the YSZ scaffold were analyzed by XRD as a function of thermal treatment. The decomposition by-products of aluminum titanate (ALT) including Al_2O_3 (Inframat 26R-0801) and TiO2 (Inframat 22N-0801A) were investigated independently as was ALT (AlfaAesar #14484) mixed with traditional NiO (AlfaAesar #12359)/YSZ (Tosoh TZ-8YS) anode powder blends. Specifically, Al_2O_3 was incorporated with NiO while TiO_2 was mixed into YSZ. These pellets had equal weights of all the constituent materials. Each combination of powders was homogenized in ethanol with an ultrasonic mixer. The solution was then set in a drying oven to allow the ethanol to evaporate. Several pellets from each batch were pressed in 2.5 cm diameter stainless steel die at 138 megapascals (MPa) weighing 2 grams each. These pellets were then sintered to up to 1400 ^{o}C at 10 ^{o}C per minute, held for one hour, and returned to room temperature at 15 ^{o}C per minute. After sintering, the dense pellets were ground in an aluminum oxide mortar and pestle and analyzed via XRD (Scintag Inc XGEN-4000). XRD scans were performed from 15 – 70 ^{o}C 2-theta at room temperature. After the initial runs were completed to evaluate the chemical interaction, NiO/ALT/YSZ pellets were sintered, then thermally treated at 800 ^{o}C for up to 150 hours under 250 ml/min of forming gas (5% H2/N2).

1.3.2 Infiltration

To analyze the effectiveness of anchoring systems, porous YSZ powders were prepared by the addition of thermal fugitives. YSZ powder, used as received, was mixed with 45 wt% cornstarch. A dispersant, ammonium polymethacrylate (Darvan C-N, RT Vanderbilt), was added at 1 wt% to ensure proper homogenization of the powder mixture. One of the powder mixtures also contained 5 wt % ALT so that both the baseline and doped mixture were prepared identically. Both slurries were placed in a centrifugal mixing device (ARE-250, Thinky Corporation) for five minutes at 1500 revolutions per minute for homogenization. The powders were prepared by freeze drying to eliminate settling of the minor dopant phase and/or thermal

fugitive. The slurries were poured directly into liquid nitrogen and flash frozen. The frozen slurry was then placed in a freeze dryer and the solvent sublimed under a 0.00532 MPa vacuum. Pellets approximately 2 grams in mass were uniaxially pressed in a 1.9 centimeter die lubricated with pressing lubricant and pressed 195 MPa. These pellets were then sintered in the furnace at 5 °C per minute up to 1450 °C, held at 1450 °C for 2 hours, and 10 °C per minute down to room temperature.

The pellets then underwent two-step infiltration process involving an intermediate low temperature heat treatment. After weighing of the porous specimens, nickel nitrate solution was dripped onto the surface of the porous pellets and allowed to infiltrate until it pooled on the sample's surface. The pellet was then placed in a vacuum chamber for five minutes to assist nickel nitrate penetration into the substrate voids. The pellet was then placed in a furnace at 500 °C for 15 minutes to decompose the nickel nitrate into nickel oxide, thus minimizing congregation of nickel nitrate to one location. After weighing to determine incremental nickel content, the process was repeated three times for each pellet. After the pellets were successfully infiltrated, they were placed in a furnace for another sintering cycle. The furnace ramped up to 1400 °C at 10 °C per minute, held at 1400 °C for 1 hour, and then returned to room temperature at a rate of 15 °C per minute to facilitate formation of the chemical anchors.

Half of the total infiltrated pellets were reduced to investigate the "as deposited" microstructure while the other halves of the pellets were subjected to long duration thermal treatment. The "as deposited" specimens were reduced at 600 ^{o}C for 5 hours to limit coarsening, while the longer duration specimens were thermally treated at 800 °C for 100 hours to mimic SOFC operation. Both specimens were reduced under 250 ml/min of 5% H_2/N_2 gas flow. Finally, both the reduced and thermally treated pellets were examined using a Field Emission Scanning Electron Microscope (FE-SEM, Zeiss Supra 55VP).

1.3.3 Cell Testing

In addition to the fundamental studies of anchoring dopants, electrochemical tests were performed to show the anchoring effects in operation. An electrolyte supported SOFC was fabricated with a 125 μm thick 8YSZ electrolyte (ESL Electro-Science, Tape 42401). The YSZ anode scaffold was applied by aerosol spraying of the slurry with and without dopant onto the anode side and sintered 1450 °C. The nickel nitrate solution from the prior infiltrations was added uniformly to the anodes. Nickel nitrate infiltration was performed as before with only 1 or 2 infiltration steps in order to exaggerate the coarsening effect. The cells were placed in a furnace and re-heated to 1450 °C for one hour to activate the chemical anchors. A common lanthanum strontium manganate cathode was then aerosol sprayed onto the cathode side and the entire cell was sintered to 1150 °C. These cells were then tested in a solid oxide fuel cell test rig at 800 °C under 250 ml/min Air and 250 ml/min N2 on the cathode, and 130 ml/min H2 on the anode side. The cells were left running under a 0.5 volt constant voltage condition for 250 hours. After testing, the cells current outputs were compared against time to show the degradation.

1.4 Results and Discussion

1.4.1 Chemical Reactivity

The anchoring process should work with ALT by allowing the zirconium from YSZ to bond with titanium from ALT and the nickel to bond with aluminum. The two reactions would yield $ZrTiO_4$ and $NiAl_2O_4$. The NiO/YSZ/ALT powder showed signs of YSZ (JCPDS 48-0224) and NiO (JCPDS 89-7131) compounds remaining, indicating that all the powder didn't react completely as seen in Figure 1. There were also peaks of $NiAl_2O_4$ (JCPDS 71-0965), $ZrTiO_4$ (JCPDS 34-0415), $AlZr_9O_{19.5}$ (JCPDS 53-0559), $Zr_{0.62}Y_{0.2}Ti_{0.18}O_{1.9}$ (JCPDS 52-1493), and TiO (89-3076). The $ZrTiO_4$ has one major peak at 30.4 degrees, which makes it difficult to identify. The NiO/ALT pellets showed peaks of NiO (JCPDS 89-7131), TiO (JCPDS 89-3076), and NiAl2O4 (JCPDS 71-0965) (Figure 2). The NiO/Al_2O_3 pellet also showed peaks of $NiAl_2O_4$ (JCPDS 71-0965) and NiO (JCPDS 89-7131) (Figure 2). The YSZ/ALT pellet had peaks of $Al_2Ti_7O_{15}$ (JCPDS 39-0052), Al_2O_3 (JCPDS 88-0826), YSZ (JCPDS 48-0224), and $AlZr_9O_{19.5}$ (JCPDS 53-0559) (Figure 3). The YSZ/TiO_2 pellet showed peaks of YSZ (JCPDS 48-0224), TiO_2 (JCPDS 89-6975), and possibly $ZrTiO_4$ (JCPDS 34-0415) (Figure 3). From the YSZ/ALT and NiO/ALT pellets, it is believed that the reaction required is sequential. Since the reaction between the NiO and Al_2O_3 of the NiO/Al_2O_3 pellet matched those of the NiO and ALT from the NiO/ALT pellet, the NiO can react with the aluminate from ALT very easily. Products of this reaction are the $NiAl_2O_4$ and remaining TiO_2. The TiO_2 can then react with the YSZ to form $ZrTiO_4$. If the YSZ is introduced to pure TiO_2, it does produce some $ZrTiO_4$, but reacting with ALT requires more energy to form these compounds. This is the reaction that will hopefully bond the substrates YSZ with $ZrTiO_4$ to some remaining ALT to $NiAl_2O_4$ and finally to the NiO, which will then be reduced to nickel metal. Figure 5 shows this anchoring pictorially. This keeps the triple phase boundary layer, which includes the path for electrons via the nickel metal, oxygen ions via YSZ substrate, and gas flow through the pores.

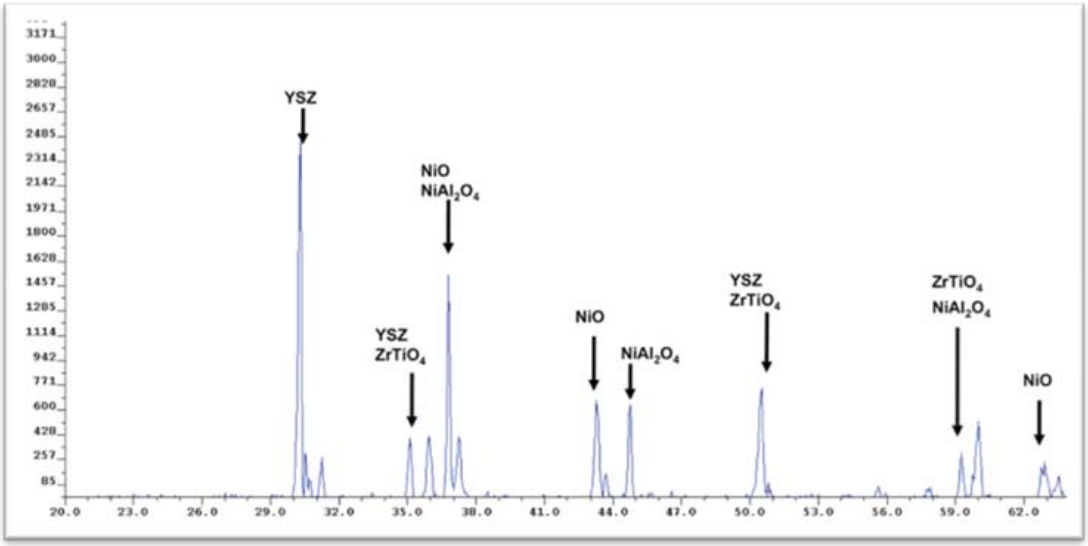

Figure 1. XRD Plot for the NiO/YSZ/ALT Powder, Indicating Unreacted Quantities of NiO and YSZ

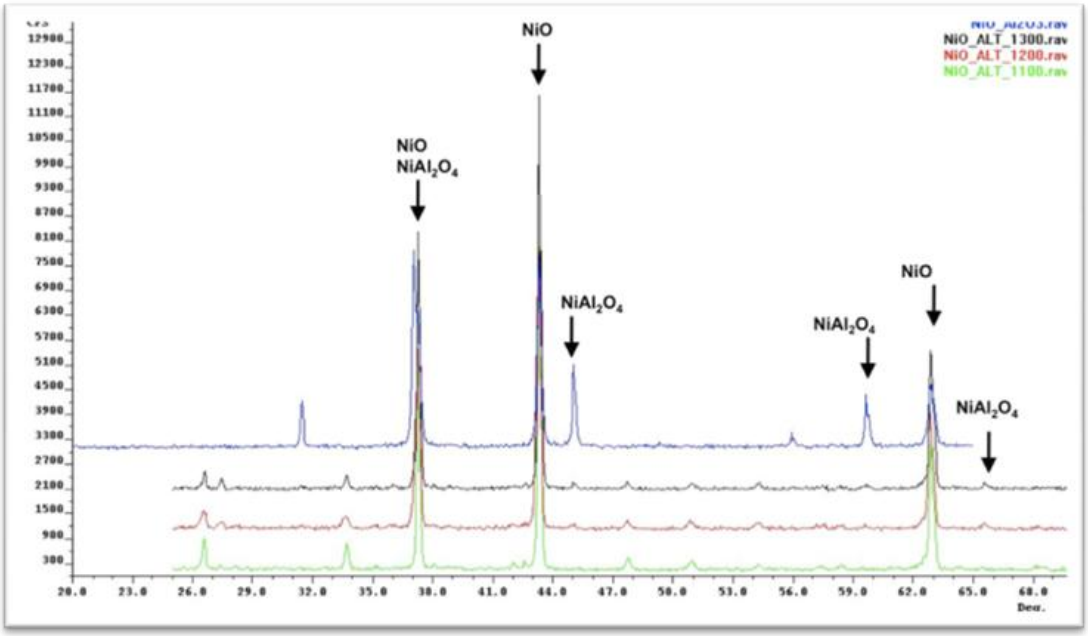

Figure 2. XRD Plots of NiO/ALT Powders for 1100 ºC, 1200 ºC, and 1300 ºC Sintering Temperatures Compared to NiO/$A1_2O_3$ Powder

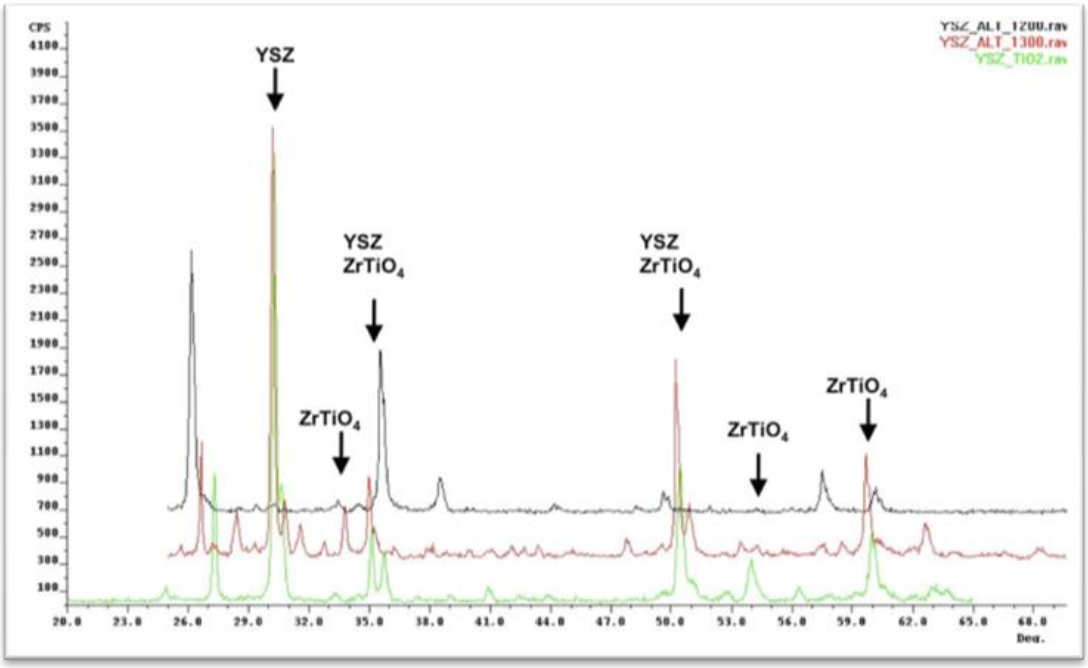

Figure 3. XRD Plots of YSZ/ALT Powders Sintered at 1200 ºC and 1300 ºC Compared to YSZ/TiO_2 Powder

1.4.2 Infiltration

The samples' fractured surfaces were examined under the field-emission scanning electron microscope (FE-SEM), noting the bottom and top surfaces. An image was taken for all samples

for the bottom, middle, and top areas of the surface. Each image also had between one and three elemental scans performed. These samples were analyzed by averaging the weight percent of nickel found by the elemental analysis in each pellet. Table 1 below shows the weight percent before and after coarsening for each sample with cornstarch thermal fugitive. From Table 1, it was evident that the ALT does help anchor the nickel to the sample, though the weights appear to be much less than that of the YSZ. This was believed to be due to the ALT acting as some type of sintering agent and reducing the pore size, thus not allowing as much nickel nitrate to penetrate the sample. From previous studies, it was determined that an infiltration of 15 wt% nickel nitrate was the optimum amount to infiltrate. After 3 cycles of infiltrate and heat treatment, little more nickel nitrate would penetrate into the sample. The weights of the final pellets compared with that of the initial pellets showed approximately 15 wt% (10 – 18 wt%) nickel metal remained in the anode. Figure 4 shows the reduced nickel on a doped and baseline sample. The effectiveness of ALT maintaining a nickel network lead to actual SOFC tests with a cornstarch thermal fugitive and ALT dopant.

Table 1. Weight Percents of Nickel in Cornstarch Samples and the Percentage of Nickel Change

Cornstarch Samples	Weight Percent of Nickel w/o ALT	Weight Percent of Nickel w/ ALT
Unreduced	76.73	39.08
Reduced	70.64	50.14
Percent of Ni Retained	-7.94	+ 28.3

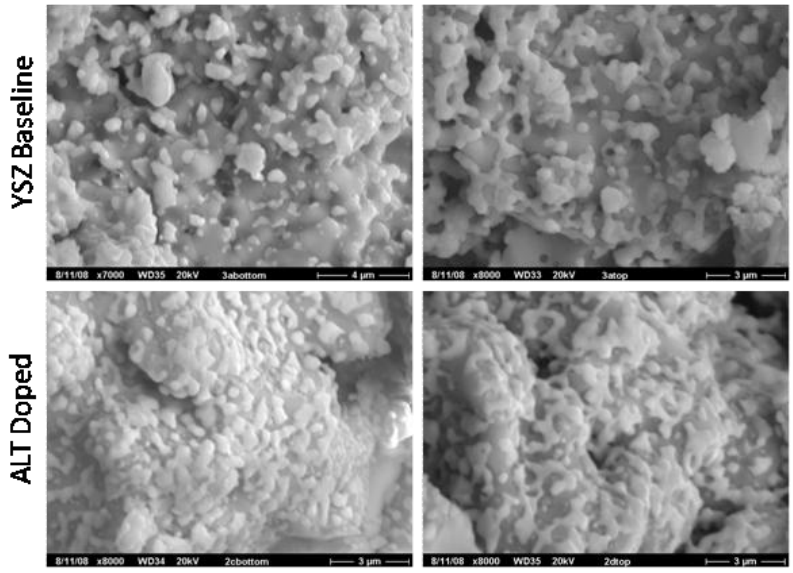

Figure 4. Micrographs of YSZ Substrate With Infiltrated Nickel After 72 Hours of 600 ºC in a Reducing Atmosphere

1.4.3 Cell Tests

The full electrolyte supported SOFC testing showed the ALT doped cells producing more power at any given time of the testing. When the third and fourth cells were re-infiltrated they were seen to yield a higher output, though the ALT doped cells were still outputting higher currents.

These can be seen in Figure 5. The current outputs of the cells with ALT dopant shown in Figure 5 were consistently higher than the undoped cells. Due to nickel congregation in the undoped samples, the oxygen ions would permeate the YSZ electrolyte and into the triple phase boundary of the anode, but a discontinuous nickel network would not allow the transmittance of the electrons to the current collector. It is apparent from Figure 5 that the anode degradation was still occurring but that the doped samples were affected less during the same period of time. While many independent parts of the SOFC test system can show degradation, all the cells were tested in the same apparatus under the same conditions with only dopants varying, thus concluding that the dopant does mitigate the nickel migration.

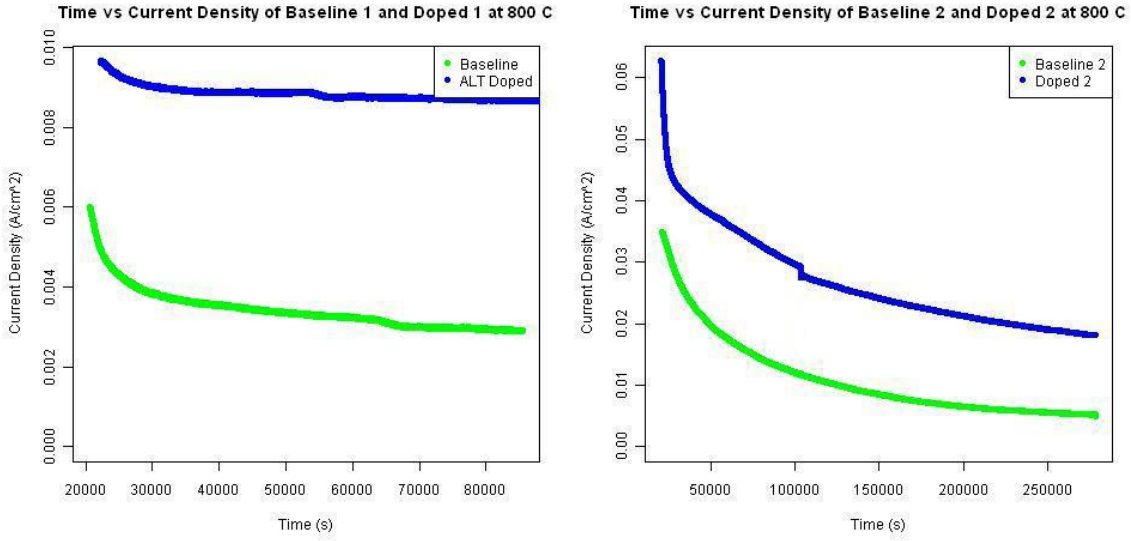

Figure 5. Electrolyte Support SOFC Tests of Infiltrated Anodes With (Doped) ALT Against Without (Baseline) ALT

A second round of testing both doped and undoped cells was conducted after re-infiltration because the low power output of the initial cell runs. The second runs indeed yield higher outputs than the first after more nickel nitrate was added to the anodes. It is believed that this acted as a second layer of nickel for the doped anode, attaching to the anchored areas of previously infiltrated nickel. Since these tests were done on electrolyte supported SOFC designs, the anodes were incredibly thin and did not allow large quantities of nickel to be infiltrated. If a thin layer of nickel oxide was present on an anchor site, the reactions could use the nickel quantity in its entirety. This nickel aluminate would still anchor the surrounding nickel but would be less conductive and act as a gap in the nickel network itself. The re-infiltration of the anode would add a second layer of nickel to these anchors and the remaining network, bridging any insulated areas. The re-infiltration also boosted the undoped cells output, though it was always less than the doped samples. As nickel nitrate was re-infiltrated and filled the gaps in the nickel network that had already begun to form from the processing of the anodes. This increased the continuity of the nickel network, but again degraded when testing began.

1.5 Conclusions

The addition of aluminum titanate (Al_2TiO_4) is shown to form a chemical anchor between the YSZ and infiltrated nickel metal in the anode of a solid oxide fuel cell. As predicted, the aluminum of ALT first must break apart and bond with the infiltrated nickel, forming nickel aluminate, before the titanium of ALT is able to bond with the zirconia of the substrate. The energy required to break apart the ALT and form new bonds was seen at temperatures as low as 1300 °C. The anchors held the nickel in a continuous network with uniform distribution during operational solid oxide fuel cell temperatures while pellets without ALT dopants had much less continuous nickel networks. Thermal fugitives, specifically cornstarch, left very nice pores to ease infiltration but combusted in a volatile manner. Further investigation into the sintering process of the anode, including thermal fugitives, is necessary for a less violent process. The quantity of thermal fugitives also needs to be further investigated. Many aspects of SOFC operation other than temperature can lead to anode migration, such as poisoning by sulfur and other contaminants. Testing on a cell or pellet with infiltrated nickel in the presence of a contaminant (ie. sulfur) require additional investigation to determine effective anchoring of nickel migration.

2.0 HIGH PERFORMANCE, HIGH POWER SENSITY SOLID OXIDE FUEL CELLS: LOAD CONTROL

2.1 Summary

This work was initiated to address the salient problem in fuel cell flight; in particular, that the variable power needed for flight cannot be addressed with a fuel cell sized to the average power requirement. We proposed to solve this problem by combining the fuel cell with a zero-average power source using power electronics. A prototype was built and data were provided demonstrating its performance. Although we are no longer aware of the key specifications of the system for which this hybrid controller is intended, it is likely that this controller could be adapted for flight testing. We strongly recommend that this be considered prior to flight test, as the capabilities of this controller would expand the flight envelope, potentially avoiding an accident.

2.2 Introduction

Figure 6 shows the basic topology of a fuel-powered propulsion system. The key components are the fuel cell, brushless DC motor, and controller. As reported previously (phase I of the project) the brushless DC motor technology is presently the most promising. Also, we have previously proposed that the most efficient steady-state topology is the one shown. This is because with proper control, the duty cycle input on the controller may be used to effectively integrate a buck-converter matching the fuel cell output with the requirements of the motor and propeller system. This avoids the expense, weight, space, inefficiency, and thermal requirements of a separate DC/DC converter.

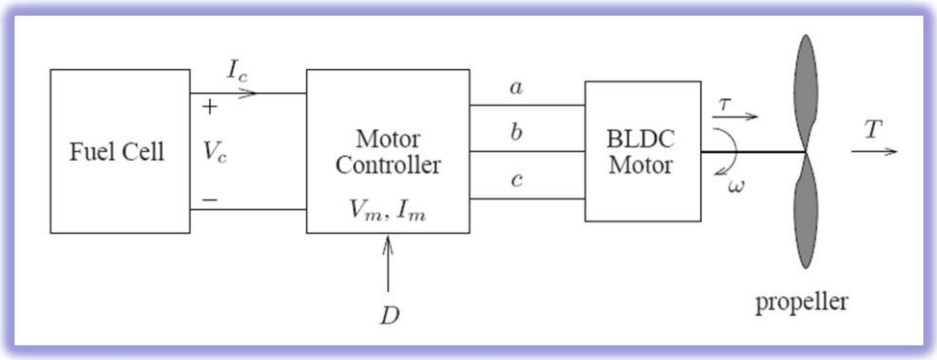

Figure 6. Fuel Cell Power Flight Propulsion System

Independent of the choice of power electronics, a fuel cell powered vehicle will operate in the steady-state at some point on its polarization curve. A typical single cell polarization curve is provided in figure 7. Of all the potential operating points on this curve, a high temperature fuel cell with a relatively small activation over-potential will operate most efficiently at roughly half the open circuit voltage. The compliant nature of the source requires power electronics with wide input voltage operating range, in comparison to systems designed to operate from battery power. Another challenge is that the propeller / motor load, when reflected to the fuel cell terminals, comprises a family of constant thrust curves that increasingly parallel

the fuel cell polarization curve at high currents. Figure 8 shows this effect. The blue line represents the linear portion of the polarization curve of a fuel cell stack, while the dashed black lines show curves of constant thrust. Note that the constant thrust curves correspond very closely to lines of constant power. The red box corresponds to a family of motor / propeller current voltage characteristics as reflected through the controller to the fuel cell terminals. Figure 8 shows a particular motor, fuel cell, and propeller combination where the duty cycle can be adjusted to change the thrust from less than 20 N to in excess of 50 N. Operating points on the right of this graph represent relatively inefficient fuel cell operating conditions that are likely outside of the design point of the balance of plant, cooling and other stack support systems. However, the increasing thrust values on the right hand side of this graph may be required to meet a given flight profile.

Our solution is to modify the IV characteristic of the fuel cell with a second source to provide a temporary increase in the flight envelope.

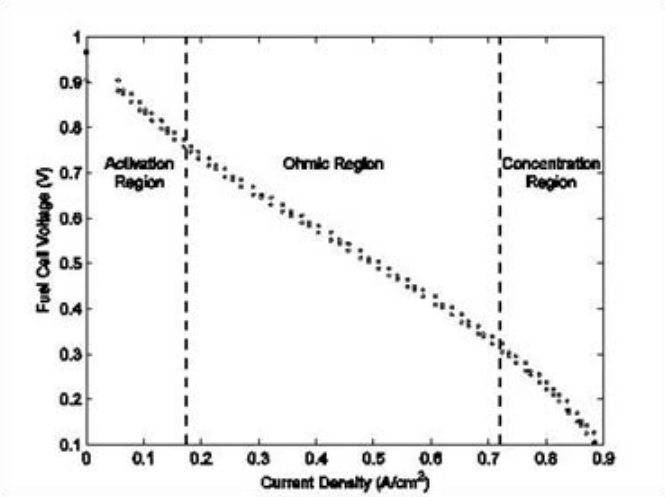

Figure 7. Typical SOFC Polarization Curve

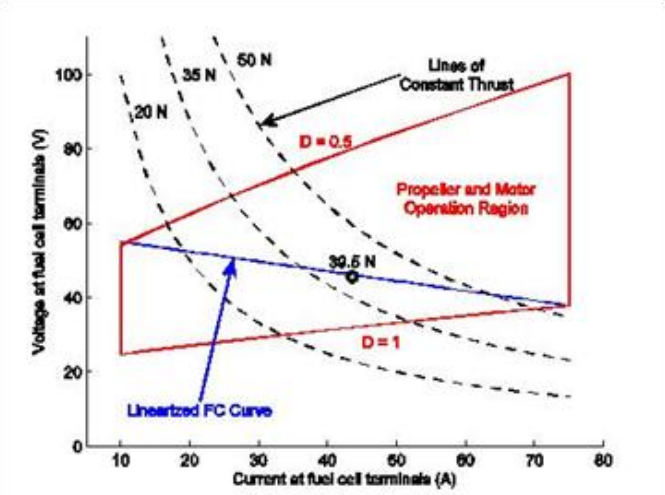

Figure 8. Thrust, Motor, and Polarizations Curves Reflected to the Fuel Cell Terminals

2.3 Methods, Assumptions, and Procedures

To provide enhanced performance, we proposed to connect a battery in parallel with the fuel cell when the fuel cell terminal voltage drops below the open circuit battery voltage. In principle, this could be accomplished by an ideal diode. In practice, we used a power MOSFET controlled to act like an ideal diode. This was done for two reasons. First, when the MOSFET is "on" it behaves like a small resistor. The loss in this resistor can be made very small by selecting an appropriate MOSFET or paralleling devices. Second, we recognize that practical operation of a hybridized fuel cell vehicle requires an energy management function to allow recharging the battery. The circuit we tested does not have this, but the topology allows energy management to be incorporated by introducing a control signal. Another nice feature of the MOSFET is that it has a body diode, which is in the correct orientation to allow hybridized operation (at reduced efficiency) in the event that the control circuit fails. We selected an IRF540 device, which has an appropriate voltage rating, a hi-performance body diode, and temperature range and other features for use in automotive power electronics. This device was controlled by an LM311 comparator. We noted that many off-the shelf high-side charge pump gate drivers are not suited to this application.

The hybrid controller was assembled and tested using a simulated fuel cell comprising an HP6012B power supply and 5 MP9100 .1 ohm 1% resistors. The battery was simulated by an HP6011A power supply. The circuit was loaded with an Agilent N3300A programmable load driven by a Tektronix AFG3022B arbitrary waveform generator. The response of the circuit was measured using a Tek DP04104 oscilloscope with ADA400A voltage and TCP0150 current probes.

2.4 Results & Discussion

Figure 9 shows the output characteristics of the hybridized source tested in our lab. The response of the system followed the polarization curve of a simulated fuel cell stack until roughly 8 amps. The green curve shows the response when the MOSFET is controlled with a comparator. After the MOSFET is turned on, the polarization curve followed the parallel combination of the battery and fuel cell curves. The blue curve shows the response when the MOSFET control circuit is disabled. In this case, which might be regarded as a fail-safe, the response is a fraction of a voltage lower. This is a result of the potential of the body diode in the MOSFET. This causes increased power loss in the MOSFET.

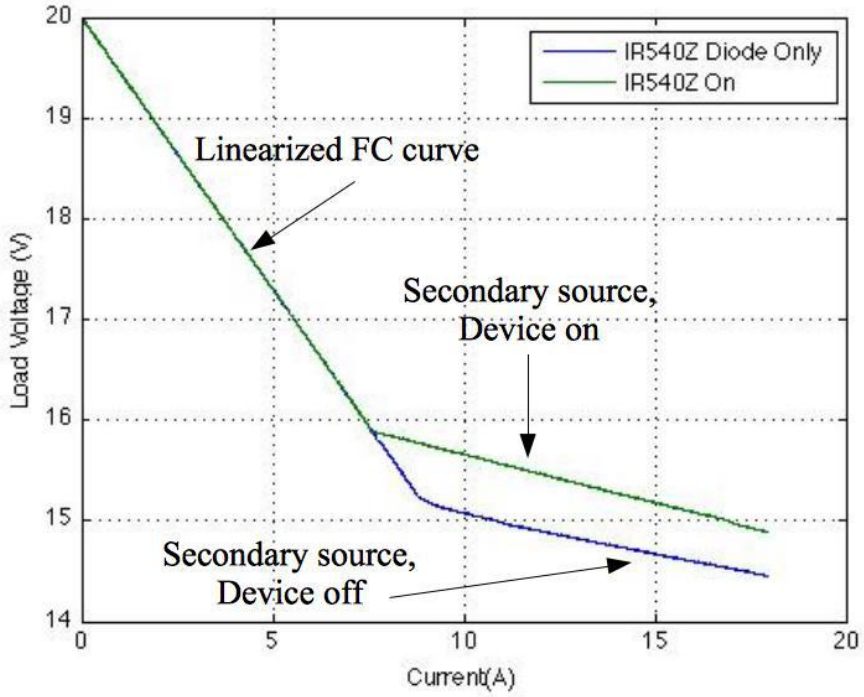

Figure 9. Current / Voltage Characteristic of Hybrid Source

2.5 Conclusions

We have demonstrated a very simple and robust means of hybridizing a fuel cell power source for flight applications. The revised shape of the source curve, figure 9, allows the propulsion system to temporarily reach thrust curves, as in figure 8, which would otherwise be inaccessible. This corresponds to an increased fight envelope.

2.6 Recommendations

Hybridization is a necessary component of any realistic fuel cell propulsion system. The system proposed here illustrates how a relatively simplistic hybridization can be achieved with low complexity. However, important work remains to integrate hybrid sources with an overall energy management control to ensure that the secondary source is recharged.

LIST OF ACRONYMS, ABBREVIATIONS, AND SYMBOLS

Acronyms & Abbreviations

SOFC	Solid Oxide Fuel Cell
MOSFET	Metal Oxide Field Effect Transistor
Vol	Volume
YSZ	Yttria-Stabilized Zirconia
CTE	Coefficient of Thermal Expansion
3-D	Three Dimensional
XRD	X Ray Diffraction
ALT	Aluminum Titanate
MPa	Megapascals
FE-SEM	Field-Emission Scanning Electron Microscope

Fuel Cell Symbols

I_C	fuel cell current (A)
V_C	fuel cell voltage (V)

Motor & Motor Controller Electric Symbols

I_m	effective motor current (A)
V_m	effective motor voltage (V)
D	duty cycle

Motor & Motor Controller Mechanical Symbols

τ	motor mechanical torque (N-m)
ω	motor speed (rad/s)

Propeller Symbols

T	produced thrust (N)